Investigating the Glacial and Topographic History of the Central Patagonian Andes using (U-Th)/He Thermochronology

Wendy De Wolf
Morse College, Class of 2014

April 30, 2014

Advisor: Mark T. Brandon
Second Reader: David Evans

A Senior Thesis presented to the faculty of the Department of Geology and Geophysics, Yale University, in partial fulfillment of the Bachelor's Degree.

Abstract

Over the past ~6 million years (Ma), large-scale glaciation has carved and shaped the Patagonian Andes. In the current interglacial period, we see high peaks and overdeepenings in the Central Patagonian Andes but only the remnants of the glaciers that formed them. This study investigates how the shape and size of the Andes has evolved since the initiation of glaciation. (U-Th)/He thermochronology, a mechanism for dating rock exhumation based on a nuclear-decay reaction, was employed to evaluate the thermal history of the topography. Thermochronometric analysis generated cooling age-elevation relationships for two overdeepenings located in the Caleta Tortel study area in Chilean Patagonia. A two-dimensional simulation demonstrated that horizontal propagation of topography is an essential factor for understanding the observed age-elevation patterns. A new three-dimensional model that simulates both horizontal propagation of surface topographic features in addition to vertical propagation relative to the surface was developed to interpret the observed age-elevation relationships. The model revealed a new explanation for the exhumation history of the Central Patagonian Andes. As the glaciers flowed over the topography, overdeepenings were incised at slow rates with topographic features propagating northward. For Fjord Steffen, the model determined a solution with a horizontal velocity of 0.3 km/Ma at an azimuth of 175° and a vertical velocity of 0.4 km/Ma. For North Cordon los Ñadis, the horizontal velocity was 0.18 km/Ma at an azimuth of 175° and the vertical velocity was 0.65 km/Ma. For East Cordon los Ñadis, the horizontal velocity was 0.25 km/Ma at an azimuth of 178° and the vertical velocity was 0.85 km/Ma. The presence of old bedrock at the surface and the slow predicted erosion rates indicate that the slow, restricted glacial movement resulted in landscape preservation. This suggests that the glacial buzzsaw effect is not active in this region.

Introduction

Glaciers are extraordinary erosive agents that shape the topography over relatively short geologic time, from a few hundred to a few million years (e.g. Shuster et al., 2011). Large and mobile, ice sheets and mountain glaciers slide across, erode, and define the landscape. While subduction results in mountain uplift, glacial erosion limits and controls the height and shape of mountains. Understanding the glacial history of a mountain range is critical for understanding the

dynamics of mountain building. Feedbacks between glaciers, climate change, and erosions ultimately determine the evolution of topography.

In this study, the glaciers that carved out the Patagonian Andes were investigated in order to elucidate the glacial and topographic history of the region. Specifically, the rate of glacial erosion and the direction of topographic propagation that formed the observed landscape were determined. Resolving this question will allow us to better understand the interaction of tectonics and erosion, a relationship that has broad implications for understanding mountain building.

To determine the exhumation and erosion that shaped the Central Patagonian Andes, (U-Th)/He thermochronology was employed. (U-Th)/He thermochronology is a mechanism for dating rock exhumation based on a nuclear-decay reaction. Surface bedrock samples were dated using this method to find the age of the modern topography. The cooling history of the topographic relief can be resolved from the resulting age-elevation profiles.

A model that simulates rock velocity towards the surface was used to interpret the age-elevation profiles. While most preceding research has only interpreted cooling age-elevation relationships with changes in vertical velocity, this study considers the possible effects of lateral propagation of topographic features in a model of rock exhumation. As rocks move from depth towards the surface, the layers do not simply move directly upward with respect to the surface topography; rock layers also have a horizontal component of motion relative to the actively eroding landform. This new model incorporates both horizontal and vertical velocities, more precisely replicating rock trajectories. By including horizontal motion, this study demonstrates that lateral propagation of features is essential to understanding how glaciers carve out relief.

Geology

The Patagonian Andes is a remarkable orogenic environment that runs along the southwestern coast of South America. The mountain range formed ~30 million years ago along a convergent plate boundary by subduction of the Nazca plate beneath the South American plate (Thomson et al., 2010). While the mean elevation of the range has remained fairly constant since 6 million years ago (Ma), relief between the peaks and valley floors has increased (Ma et al., in review). Mountain glaciers and continental ice sheets carved deep U-shaped valleys and fjords, magnifying the relief between the valley and peak. There is a about a 5 kilometer difference in elevation between the tallest peak and the lowest fjord in Patagonia. Standing at 4059 meters, the summit of

Cerro San Valentin is the highest point in Chilean Patagonia. By contrast, nearby Canal Baker and Canal Messier are the second and fourth deepest fjords in the world. Canals Baker and Messier are -1344 meters and 1468 meters below sea level. Lago General Carrera/Buenos Aires, a large freshwater or inland fjord, has a depth of 360 meters below sea level. These glacial overdeependings are compelling evidence of active and powerful glacial activity in the area. Widespread glaciation in Patagonia initiated between 7 and 5 Ma (Mercer et al, 1982). The conventional inference, however, is that the majority of glacial erosion occurred in the last 2 Ma, concurrent with late Cenozoic global cooling (Egholm et al., 2009).

The west side of the central Patagonian Andes has high precipitation rates, reaching up to 6000 mm/year (Smith and Evans, 2007). Saturated winds coming across the Pacific are pushed up the side of the mountain range, producing orogenic precipitation. Thus, there is ample and steady source of water to promote glacial growth in the region. The mountains act as a rain shadow for the eastern side of the range, which is a dry environment. The dry east side ensures the preservation of the oldest mountain glaciations (Mercer et al, 1982).

Glacial History

Brozovic et al. (1997) proposed that glacial processes restrict the elevation, relief, and topographic development of mountains. Glacial activity is a climatic limit on landscape development, independent of the rate of tectonic processes. The results suggested that glacial erosion is the dominant factor controlling maximum mountain height above the equilibrium level altitude (ELA). The equilibrium level attitude marks the boundary between glacial ablation and accumulation. This concept that the glacial erosion controls topography above the ELA regardless of rock uplift rate is termed the "glacial buzzsaw" effect. As a result of the buzzsaw, the mean elevation of the orogen is located at the mean ELA (Thomson et al., 2010). Subsequent research identified the glacial buzzsaw effect operating on mountain ranges across the world.

Thomson et al. (2010) found an exception to this glacial buzzsaw hypothesis in the Patagonian Andes. In the southern latitudes (49° S to 56° S), glacial activity promotes constructive growth of the orogen's height and width. Thomson et al. concluded that the glacial buzzsaw effect broke down south of approximately 45° S, where the mean elevation of the mountain was far above the mean ELA. The presence of old cooling ages at the surface (>10 Ma) implies inefficient regional glacial erosion. While the glaciers are warm-based glaciers capable of erosive action, glacier

basal flow is restricted so that the landscape is preserved. Previously, glacial preservation of landscapes had only been observed in connection with cold-based glaciers that do not slide (Thomson et al., 2010).

In a recent paper, Ma et al. challenged the general assumption that glacial erosion was limited to the last 2 Ma (Egholm et al., 2009) and suggested that the Patagonian Andes have experienced long-term erosion. Ma et al. (in review) argued that large ice cap glaciations were present in Patagonia as early as 6 Ma, cutting the landscape at a slow rate over a longer period of time. The size of early glaciations was estimated using a numerical ice model and the provenance of granitic cobbles in glacial deposits on the east side of the Andes. The ice model simulated glacial activity that could transport granitic cobbles from the Patagonia batholith on the west side of the range to the deposits on the east side of the range. According to over 200 simulations, Ma et al. determined that large ice caps completely covered the bedrock topography at ~10 Ma. Furthermore, the results indicate that in order for the granitic cobbles to be deposited on the east side of the range, there was low relief prior to the initial glaciation. While carrying the granitic cobbles, the immense ice sheets carved the deep valleys.

Thermochronology

This research further investigates the rate of glacial erosion, illuminating the glacial and orogenic development of the Patagonian Andes using (U-Th)/He thermochronology. Thermochronology is a technique for dating the thermal history of a mineral that extracts information about the timing of rock exhumation (*Quantitative Thermochronology,* Braun, 11). At high temperatures, isotopic systems in the bedrock are open systems and daughter products rapidly diffuse out. At a specific low temperature, the isotopic system becomes closed and all daughter products are retained in the host mineral. This transition where the isotopic system shifts from open to closed is identified as the closure isotherm. The closure isotherm is more accurately described as a partial retention zone, the zone over which the system becomes closed (Reiners and Brandon, 2006). The thermochronological clock begins when the host mineral passes through this closure isotherm and thus at the closure isotherm, minerals have a cooling age of 0 Ma (Dodson, 1973). The cooling age of the mineral at the surface corresponds to the time since the mineral passed through the closure isotherm. (*Quanitative Thermochronology*, Braun, 14). (U-Th)/He

thermochronology is based on the nuclear decay-reaction of $^{(235,238)}U$, ^{232}Th, and ^{4}He in apatite minerals after passing through a low closure temperature of about 65° (Reiners and Brandon, 2006).

A bedrock surface that has the same cooling age across all points is called an isochrone. An isochrone is formed as rock passes through the closure isotherm. In the past 15 years, there have been advances in both understanding and utilizing the relationship between surface topography and thermochronology. For thermochronological systems with low closure temperatures, including apatite (U-Th)/He thermochronology, the cooling ages are linked to and elucidate the surface topography at the time of closure. Considering the isochrones as a form of stratigraphy, the long-term exhumation and erosion of the bedrock surface can be deduced (McPhillips and Brandon, 2010). Shallow isochrones resemble a muted image of the surface topography and therefore can be used to investigate changes in relief.

In the Patagonian Andes, a large number of ages have been determined from thermochronometric dating of bedrock samples, 755 of which give reliable ages. Figures 1 is a map of the Central Patagonian Andes, indicating thermochronological sample locations from previous field studies. A variety of thermochronolgical systems have been used including helium zircon (HEZ), helium apatite (HEA), fission track zircon (FTZ), and fission track apatite (FTA). Thomson et al. (2010) sampled in the Caleta Tortel study area in Chilean Patagonia. The study reported 246 new apatite (U-Th)/He ages and 136 apatite fission tract ages for samples collected along the Patagonian Andes from 38° S to 56° S. Cooling ages from Thomson et al. (2010) indicate that the topography spans about 10 Ma.

Figure 1 Map of Patagonia including all existing thermochronometric data

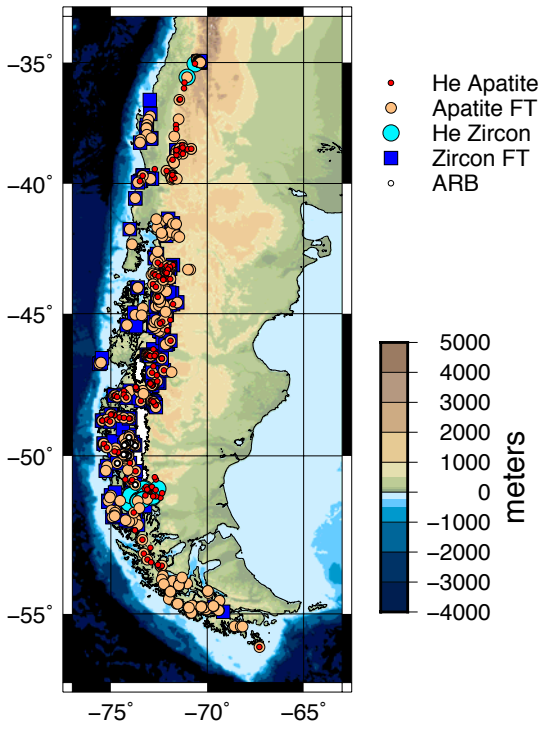

Following Thomson et al. (2010), Guillaume et al. (2013) collected samples in the same region of the Central Patagonian Andes. Using HEA thermochronology, age-elevation plots were produced for four transects at latitudes ranging from 45°S to 28°S. Guillaume et al. (2013) investigated if the opening of the slab window influenced the low erosional rates at latitudes south of 49°S, which Thomas et al. (2010) ascribed to glacier protection. In evaluating the ages of the samples, Guillaume et al. deduced thermal histories from a similar inverse modeling system using the rate of vertical motion as the only variable. Neither Thomson et al. nor Guillaume et al. incorporated horizontal propagation into their model. They use a stacked age-elevation approach, assuming that the isotherms are layered directly above the closure isotherm.

In this study, new transects were collected in the same region to evaluate further the thermal history and infer the glacial erosion of the Central Patagonian Andes. The samples were analyzed using similar HEA thermochronology methods as used by Thomson et al. and Guillaume et al. Unlike the previous studies, horizontal propagation of landforms as well as vertical rock uplift was included in the modeling system to reconstruct the evolution of topography. According to this

revised modeling technique, new conclusions were determined for the rates of glacial erosion in Patagonia.

Study Area

In December 2012, we traveled to the Caleta Tortel study area in Aysen Province, Chile to collect new samples for thermochronological analysis. The remote region is about 400 km south of the Coyhaique, the capital of the province, along a one-lane dirt highway. The study area lies in the center of the Patagonian Andes, characterized by spectacular summits, deep valleys, and fathomless fjords. The landscape is a remarkable example of a dynamic orogenic environment. The Chile triple junction, where the Nazca, Antarctic, and South American Plates collide, is located right adjacent to the study area. Accordingly, there is especially active subduction and uplift in this region. The Northern Patagonian Ice Sheet bounds the study area directly to the north and the Southern Patagonian Ice Sheet extends south of the region. The bedrock in the region is the granitic Patagonian Batholith, containing apatite minerals that can be dated using thermochronology.

Samples were collected at two sites on the west side of the range just south of the Northern Patagonian Ice Field. The sites were located between 72° and 75°W and 46° and 47°S. According to the results from Thomson et al. (2010), we purposely chose sampling sites south of 45° S. Cordon los Ñadis is a high peak, reaching a summit of 1780 meters, located northeast of the village of Caleta Tortel along the Rio Baker. Fjord Steffen is a glacial overdeepening directly south of the Northern Patagonian Ice Field. The town of Caleta Tortel is situated on the southeast bank of the Fjord, at the mouth of the Rio Baker. Two transects were performed along the walls of the Fjord Steffen and one transect at Cordon los Ñadis. After climbing to an elevation of approximately 1,000 meters, samples of the bedrock were collected about every 150 meters on the descent. In total, 35 samples were collected during the field season. Figures 2 and 3 are maps of the study areas, showing the locations of the samples

Figure 2 Map of Fjord Steffen Study Area

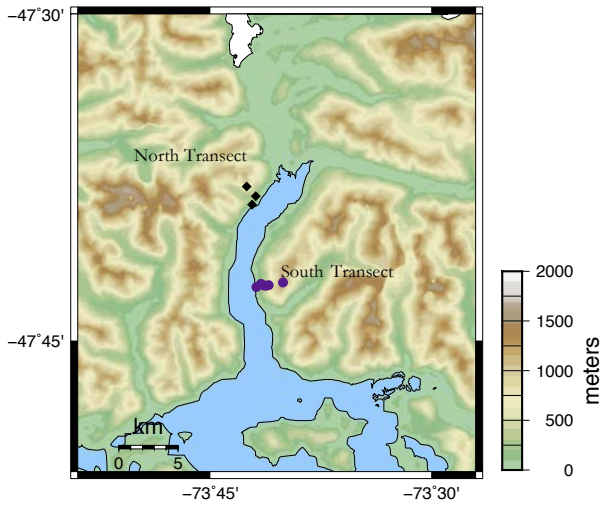

Figure 3 Map of Cordon Los Ñadis Study Area

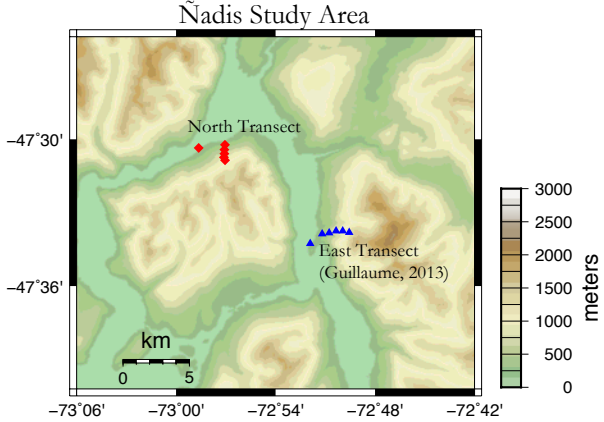

Methods

(U-Th)/He Thermochronologic Analysis

The cooling ages of the collected samples were determined using (U-Th)/He thermochronology. When a rock surface passes through the closure isotherm, the system becomes closed and daughter products of nuclear-decay reactions are retained within the mineral. (U-Th)/He thermochronology measures the build up of ^{4}He that has decayed from $^{(235,238)}U$ and ^{232}Th in apatite minerals (Reiners and Brandon, 2006). Based on the concentrations of these elements in a bedrock sample, the cooling age of the rock can be determined. The cooling age corresponds to the time at which the mineral passed through the closure isotherm (Dodson, 1973).

(U-Th)/He thermochronology is a useful system for evaluating the evolution of topography (e.g. Braun et al., 2002). Helium in apatite grains has a low closure temperature, approximately 65°C, and thus the closure isotherm for this system is only approximately 3 kilometers in depth (Reiners and Brandon, 2006). Because the closure isotherm is near the surface, it closely mimics the surface topography. Isochrones, consequently, resemble the surface topography at the time the surface passed through the closure isotherm (Braun, 2002). The isochrones are linked to and therefore elucidate the modern surface relief.

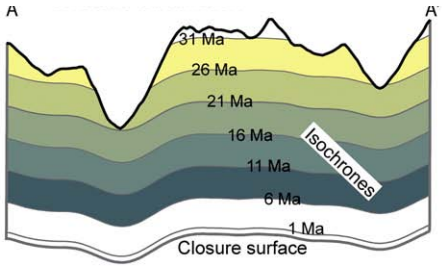

Figure 4 Cross section of relatively flat isochrones, assuming constant exhumation rate and constant topography (From McPhillips and Brandon, 2010)

To prepare the samples for thermochonological analysis, the apatite grains were isolated from the granite samples. Each sample weighed approximately 3 to 4 kilograms. In the Yale University rock laboratory, the samples were crushed into coarse gravel with the chipmunk crusher and then into fine sand with the disk mill. The fine sand was filtered through a 32-mesh 500-micron sieve with a ro-tap. At John Garver's laboratory at Union College, the sands underwent physical mineral separation on a Gemini shaking table. The shaking table separates the sand grains by density. The separate fraction was suspended in heavy liquids, separated further by density. Then, the separate fraction was put through the Franz Isodynamic Seperator, which separates samples by magnetism. From the separate fraction, apatite grains were individually picked. Approximately 0 to 5 grains were picked per sample.

At David Shuster's laboratory at the Berkeley Geochronology Center, each individual grain was heated to 1000°C with a laser in an enclosed machine. At this high temperature, the grain releases gases, including ^{4}He. Then, the enclosed gases were spiked with a known amount of ^{3}He. While the absolute concentration of ^{4}He cannot be measured directly, the ratio between a known amount of ^{3}He to ^{4}He can be determined. The raw calculation assumes that there is uniform distribution of the parent and daughter in the grain. If decay occurs in the outer 12 microns of a grain, however, the alpha particle (^{4}He) can be ejected out of the grain. To account for the lost material, a correction factor is included in the calculations. If this loss of helium were not accounted for, the grain would seem younger than its true age (Farley et al., 1996). Many of the picked grains were broken, necessitating a length correction before the alpha ejection calculation; the original length was set to 1.5 times the broken length of grain (Ehlers and Farley, 2002). Grains were carefully screened for the presence of zircon inclusions in the apatite grains, which can also bias the measurements. Zircon has a much higher concentration of uranium and thorium relative to those

for apatite. Small zircon inclusions can increase the amount of helium in the grain and make the grain appear older than its true age.

Uranium and thorium are more retentive in apatite than helium and thus once the grains are degassed, the remaining solid still contains the original concentrations of uranium and thorium. The ispotopic concentrations of uranium and thorium in the grain was determined by mass balance. The remaining solid was put in a Teflon tube and dissolved in water and nitric acids to extract the uranium and thorium. A known amount of ^{233}U was added and the ratios of uranium and thorium to ^{233}U were measured using inductively coupled plasma mass spectrometry (ICPMS).

The final data set includes a set of locations, defined by coordinates and elevation, with corresponding helium apatite (HEA) cooling ages. Table 1 includes the accepted HEA cooling ages for all samples from this study and from Guillaume (2013). Due to large errors or unreasonable age results, certain grain ages were rejected. If all grain ages were rejected, then the sample was excluded from analysis. For each sample, the accepted grain ages were averaged to one single value. The data was distilled to an age vs. elevation plot, representing the ages of the bedrock surfaces along the valley wall from sea level towards the summit. Figures 6 and 7 are the age-elevation relationships for transect from Fjord Steffen and Cordon los Ñadis. The slope of this curve describes the exhumation rate of the landscape, assuming a flat, unchanging closure isotherm.

Modeling Age-Elevation Relationships (AER)

A computational simulation was constructed that models the uplift of isochrones to the modern bedrock surface and generates an associated age-elevation plot. Using a reductionist strategy, the uplift of topography is simplified to the relationship between rock velocity vectors and isochrones. A two-dimensional model was developed to understand the fundamental behavior of the system. This basic geometric approach demonstrates the behavior of end-member cases for the shape of the closure isotherm. A three-dimensional model incorporated the topography of Patagonia and evaluated the behavior of the locations where the samples were collected.

The two-dimensional example represents surface topography as a Gaussian surface. The model assumes that the closure isotherm is a perfect image of the surface, stacked directly below the surface. The surface landform remains fixed in the model while the rock progress through the system. The rock is advected through the closure isotherm, forming isochrones that exactly mimic the shape of the closure isotherm. The exhumation rate is defined not only by a vertical velocity but

also by a horizontal velocity. Consequently, the rock moves up obliquely before reaching the surface landform. The program takes a Gaussian surface and translates it directly down to form the closure isotherm. The closure isotherm is translated up at the material velocity to form a series of isochrones. Figure 5 is a schematic demonstration of the basic procedure for the simulation. The age of the bedrock surface is determined by the isochrones that intersect it. By changing the direction of the material velocity vector, the age-elevation patterns for end-member cases of dynamic uplift can be generated.

Figure 5 Basic procedure for the two-dimensional simulation. 5a represents rock uplift parallel to the slope, with negative horizontal propagation. 5b represents rock uplift across the slope, with positive horizontal propagation.

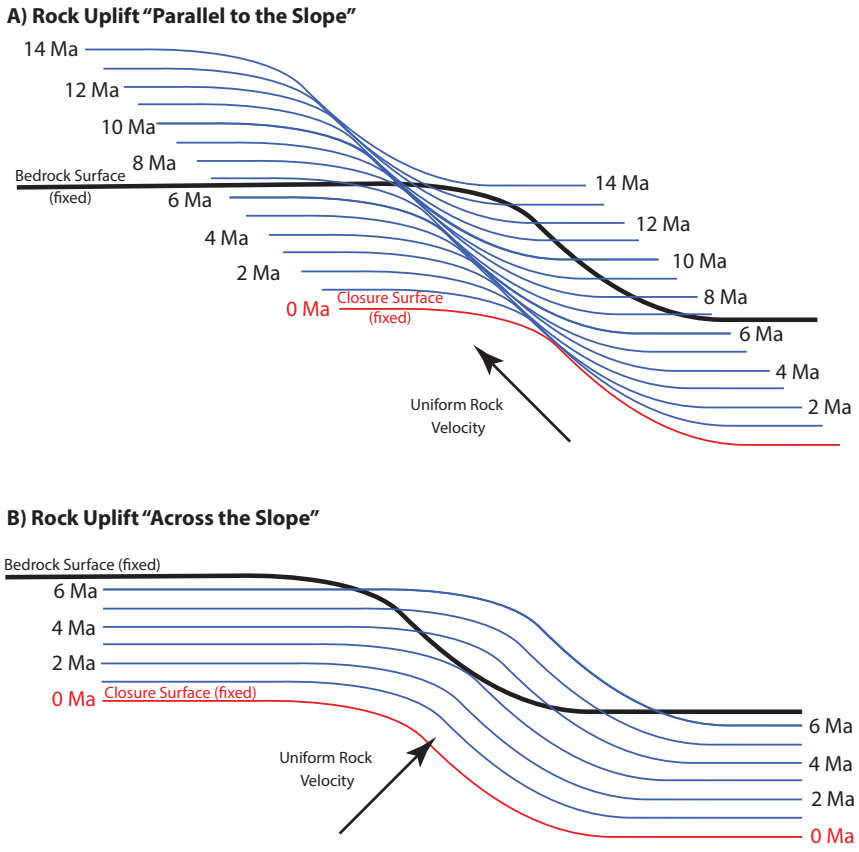

While the two-dimensional simulation is a useful tool for illustrating how isochrones are exposed during vertical and lateral erosion, it does not account fro the evolution of three-dimensional landforms. The three-dimensional simulation applies similar modeling techniques to

actual topographic cases. The input for the three-dimensional simulation is a DEM (digital elevation model) map of Fjord Steffen or Cordon los Ñadis, the two primary sampling locations from our fieldwork.

The program takes the modern topography and translates it directly down 3 kilometers to form the closure isotherm. The material velocity vector relative to the landform is defined by three components: the vertical velocity, the horizontal velocity, and the azimuth of the velocity vector (the orientation of the horizontal projection of the vector relative to north). The horizontal component of the material velocity vector relative to the east (x) is defined by the sine of the azimuth and the horizontal component of the material velocity vector relative to the north (y) is defined by the cosine of the azimuth. The rate of vertical uplift (z) is equivalent to the exhumation rate or the erosion rate.

Results

Thermochronology

Of the 32 samples collected, 21 contained datable grains. Four of these 21 samples were rejected because the cooling ages had large errors or could not be replicated. Only 3 of the samples from the North Fjord Steffen transect produced replicated grain ages. Our analysis incorporated data from a study by Guillaume (2013), which was also collected in the Cordon los Ñadis area. For Fjord Steffen, cooling ages were between 5 and 11 Ma, indicating slow exhumation rates. For the Cordon los Ñadis area, cooling ages ranged from 4 to 8 Ma. The age-elevation relationships reveal no linear increase of age with elevation but instead a complex scatter of ages. Figure 6 is the age-elevation relationship for Fjord Steffen and figure 7 is the age-elevation relationship for Cordon los Ñadis. Table 1 includes all data from thermochronometric analysis of the samples.

Figure 6 Age-elevation relationship for Fjord Steffen

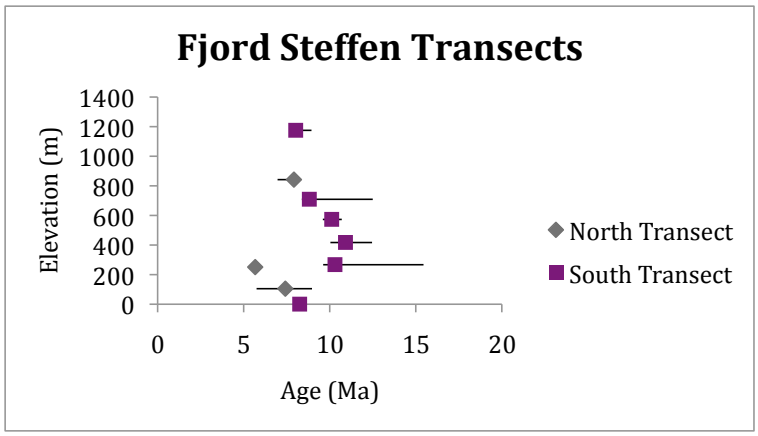

Figure 7 Age-elevation relationship for Cordon los Nadis including samples from this study and from Guillaume 2013.

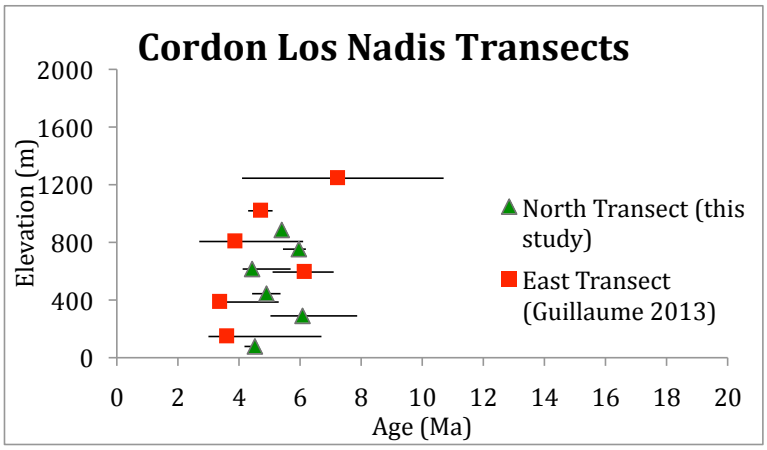

Sample name	Latitude	Longitude	Elevation	Age of Weighted Average (Not including rejected ages)	Standard Err (Ma)	Min Age	Max Age	Location
FS16	47.70908	73.69784	0	8.23	0.14	8.07	8.39	Fjord Steffen Southern Transect
FS14	47.70662	73.69276	267	10.28	0.10	9.62	15.45	Fjord Steffen Southern Transect
FS13	47.70799	73.68935	417	10.89	0.10	10.04	12.46	Fjord Steffen Southern Transect
FS12	47.70814	73.68685	573	10.09	0.07	9.60	10.70	Fjord Steffen Southern Transect
FS11	47.70767	73.68395	709	8.79	0.05	8.38	12.50	Fjord Steffen Southern Transect
FS08	47.70565	73.66784	1175	8.00	0.08	7.86	8.94	Fjord Steffen Southern Transect
FS06	47.63965	73.69865	251	5.67	0.05	5.51	6.05	Fjord Steffen Northern Transect
FS02	47.63228	73.70897	842	7.92	0.09	6.97	8.03	Fjord Steffen Northern Transect
FS17	47.64607	73.70287	105	7.42	0.13	5.75	8.97	Fjord Steffen Northern Transect
CLN07	47.5059	72.97732	78	4.52	0.06	4.18	4.63	Cordon Los Nadis
CLN05	47.50379	72.95094	290	6.08	0.07	5.03	7.87	Cordon Los Nadis
CLN04	47.50712	72.95153	444	4.90	0.04	4.43	5.36	Cordon Los Nadis
CLN03	47.50985	72.95151	615	4.43	0.03	4.12	5.69	Cordon Los Nadis
CLN02	47.51231	72.95196	753	5.96	0.03	5.44	6.19	Cordon Los Nadis
CLN01	47.51434	72.95079	886	5.40	0.05	5.32	5.53	Cordon Los Nadis
Guillaume2013_DES17-A	-47.5635	-72.826	1245	7.22	0.73	4.1	10.7	Cordon Los Nadis
Guillaume2013_DES18-A	-47.5625	-72.8325	1019	4.70	0.32	4.30	5.10	Cordon Los Nadis
Guillaume2013_DES19-A	-47.5625	-72.8392	806	3.86	0.25	2.70	6.10	Cordon Los Nadis
Guillaume2013_DES20-A	-47.5638	-72.8462	594	6.13	0.28	5.10	7.10	Cordon Los Nadis
Guillaume2013_DES21-C	-47.5645	-72.8532	386	3.36	0.19	3.20	5.30	Cordon Los Nadis
Guillaume2013_DES22-A	-47.5711	-72.8652	147	3.59	0.14	3	6.70	Cordon Los Nadis

Table 1 (U-Th)/He Thermochronlogy Data for All Samples
For each sample, the location is defined by latitude, longitude, and elevation. The age of each sample is the weighted average of all of the youngest ages in that sample. The minimum and maximum ages determined by subtracting or adding the standard error to the weighted average.

Two-Dimensional Simulation

The two-dimensional simulation was run with three different horizontal velocities that represent end-member cases. In the first case, the horizontal velocity was set to a positive exhumation (at an angle to the right of the vertical axis) across the slope of the modern bedrock surface. Figure 8 illustrates the contoured isochrones and figure 9 shows the continuous isochrones generated by this exhumation angle. The resulting age-elevation relationship is C-shaped, revealed in figure 10. In the second case, the horizontal velocity was set to 0 km/Ma, resulting in a vertical material velocity (90° angle relative to the horizontal). Figure 11 illustrates the contoured isochrones and figure 12 shows the continuous isochrones generated by this vertical material velocity. The resulting age-elevation relationship is a straight vertical line, revealed in figure 13. In the third case, the horizontal velocity was set to a negative exhumation (at an angle to the left of the vertical axis) parallel to the topographic surface. Figure 14 illustrates the contoured isochrones and figure 15 shows the continuous isochrones generated by this exhumation angle. The resulting age-elevation relationship is 7-shaped, revealed in figure 16.

Figure 8

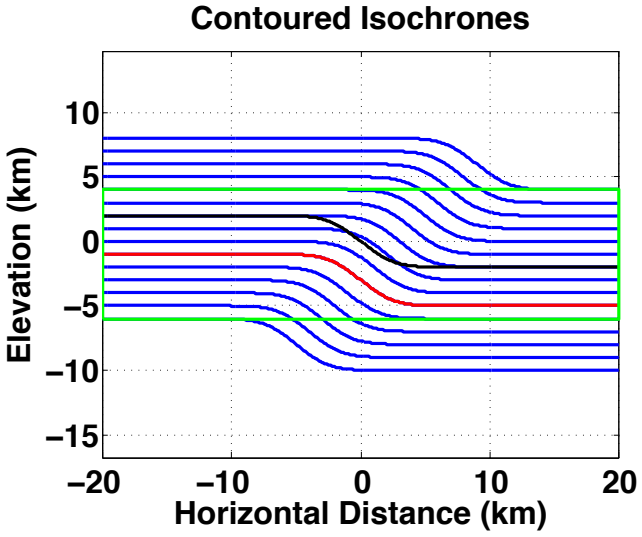

Figure 9

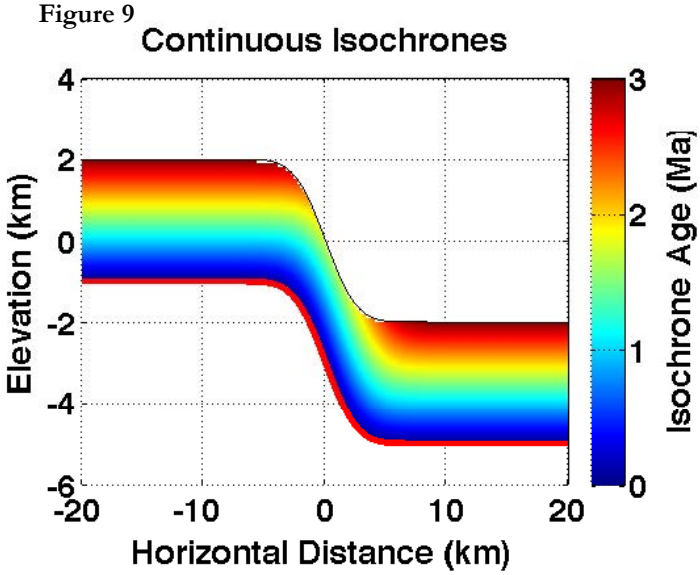

Figure 10

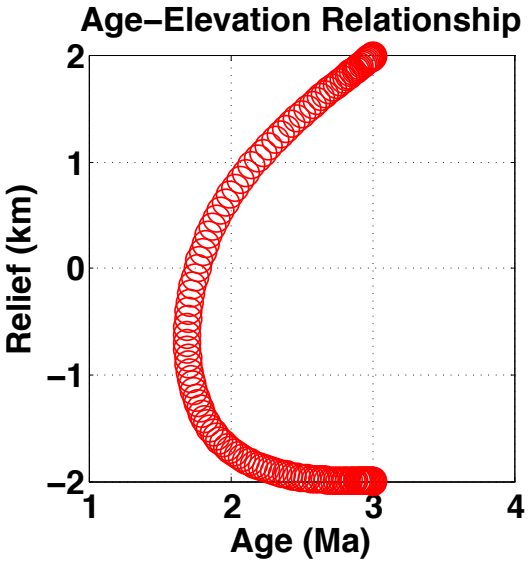

Figure 8 illustrates the contoured isochrones generated by a positive angle of exhumation. The black line represents the surface relief, the red line represents the closure isotherm, and the blue lines represent the isochrones. **Figure 9** illustrates the continuous isochrones generated by a positive angle of exhumation. **Figure 10** demonstrates the C-shape age-elevation relationship resulting from a positive angle of exhumation.

Figure 11

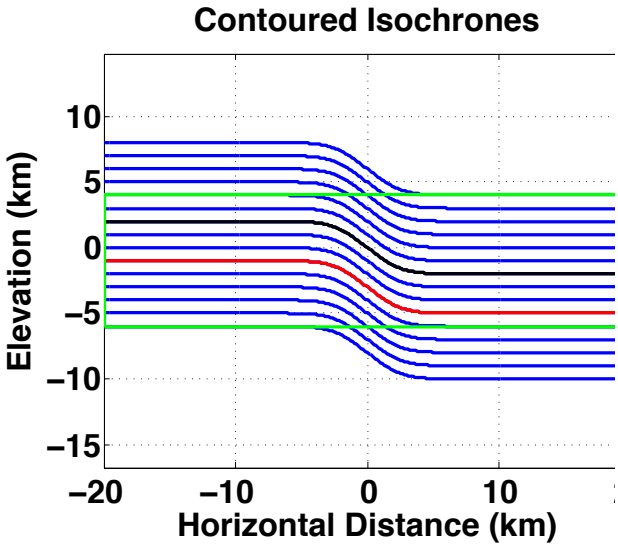

Figure 12

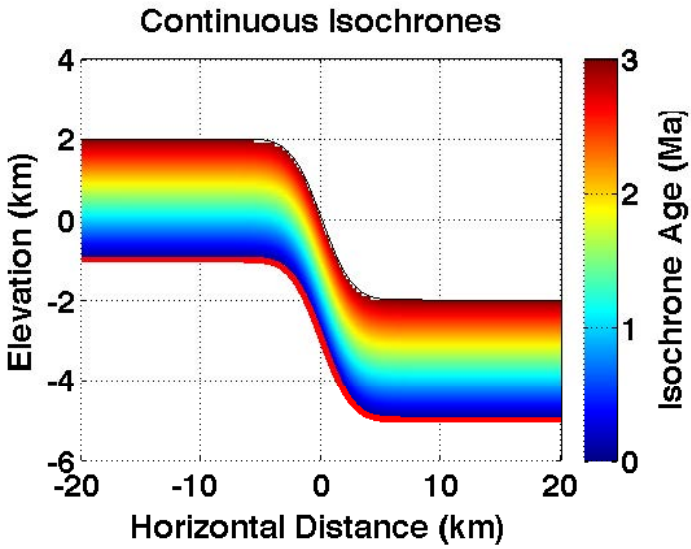

Figure 13

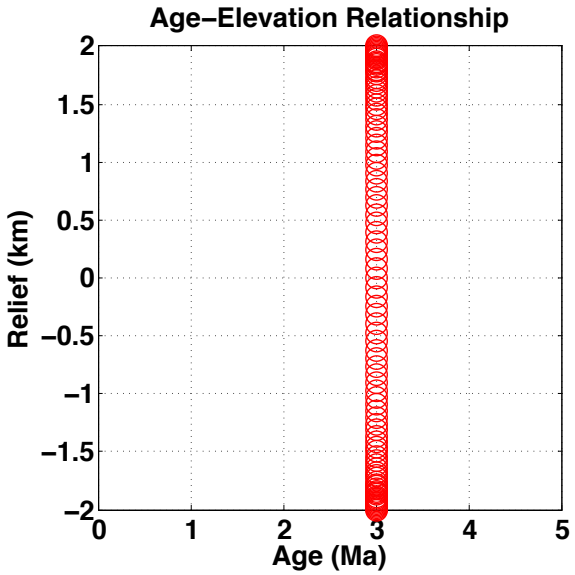

Figure 11 illustrates the contoured isochrones generated by a 90° angle of exhumation. The black line represents the surface relief, the red line represents the closure isotherm, and the blue lines represent the isochrones. **Figure 12** illustrates the continuous isochrones generated by a 90° angle of exhumation. **Figure 13** demonstrates the straight-line age-elevation relationship resulting from a 90° angle of exhumation.

Figure 14

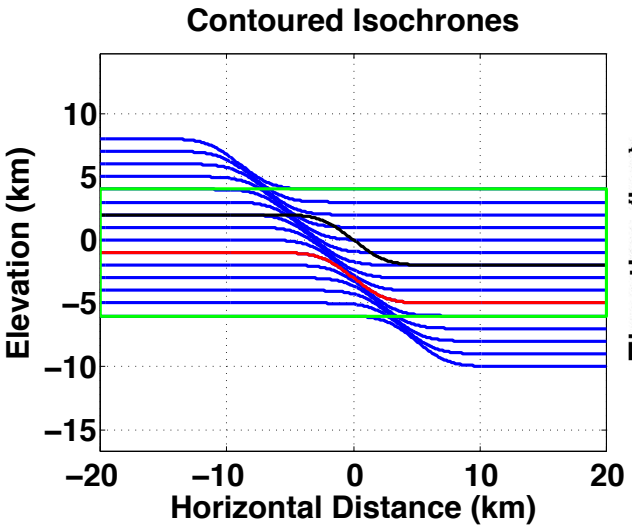

Figure 15

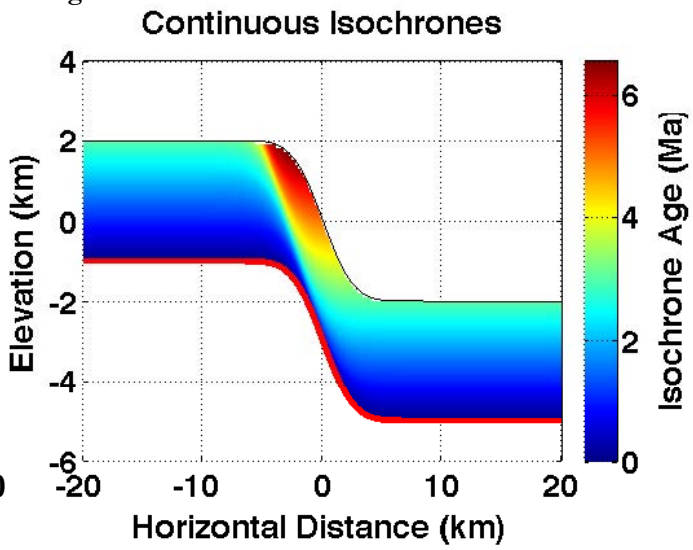

Figure 16

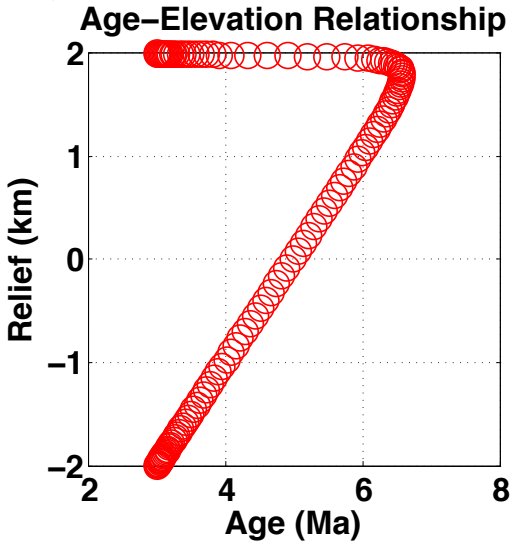

Figure 14 illustrates the contoured isochrones generated by a negative angle of exhumation. The black line represents the surface relief, the red line represents the closure isotherm, and the blue lines represent the isochrones. **Figure 15** illustrates the continuous isochrones generated by a negative angle of exhumation. **Figure 16** demonstrates the 7-shape age-elevation relationship resulting from a negative angle of exhumation.

Three-Dimensional Simulation

The three-dimensional simulation produces three figures for each given material velocity vector. The first figure is a map of the landscape surface that indicates the age of every point using a color scale. The second figure includes an age-elevation plot for the observed ages of our samples and an age-elevation plot for the predicted ages of our samples based on the model. The third figure is a plot of the observed age versus the predicted age. If the points fall along a 1-to-1 plot, the model correctly simulates the observed topography. By adjusting the horizontal velocity, the angle of inclination, and the vertical velocity of the model, the actual behavior of the topography can be determined.

The Cordon los Ñadis data set includes samples collected by Guillaume from Université de Rennes in 2013, identified as the East Cordon los Ñadis Transect. The Fjord Steffen data only includes transects from our fieldwork. There are distinct solutions for the Fjord Steffen transect, the North Cordon los Ñadis transect, and the East Cordon los Ñadis transect. The uplift dynamics vary for these different locations because they are each located in distinct overdeepenings.

For Fjord Steffen, the horizontal velocity was 0.3 km/Ma at an azimuth of 175° and the vertical velocity was 0.4 km/Ma. Figures 17, 18, and 19 illustrate the model results for Fjord Steffen. For East Cordon los Ñadis, the horizontal velocity was 0.18 km/Ma at an azimuth of 175° and the vertical velocity was 0.65 km/Ma. Figures 20, 21, 22 show the model results for East Cordon los Ñadis. For North Cordon los Ñadis, the horizontal velocity was 0.25 km/Ma at an azimuth of 178° and the vertical velocity was 0.85 km/Ma. Figures 23, 24, and 25 demonstrate the model results for North Cordon los Ñadis. For all of the solutions, the simulation is less precise at reproducing the observed data at mid elevations between approximately 300 and 600 meters.

Figure 17

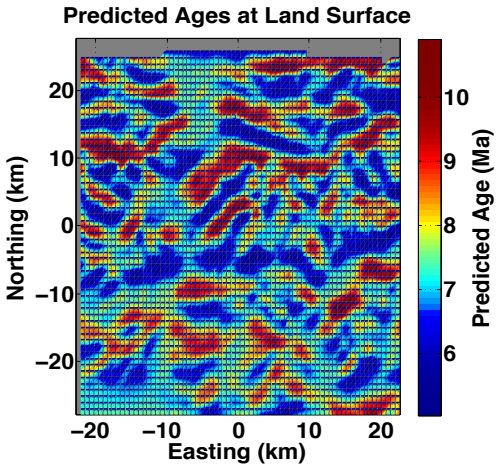

Figure 18

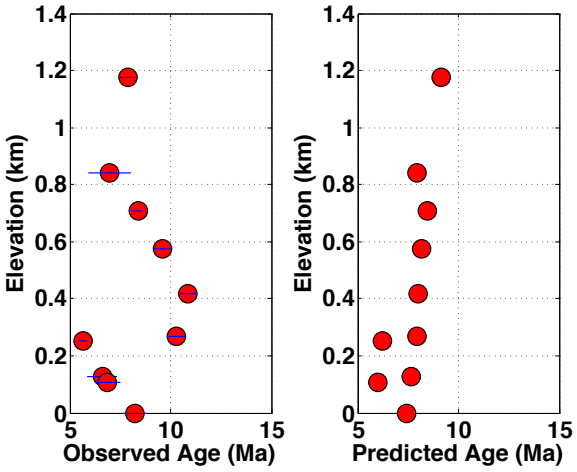

Figure 19

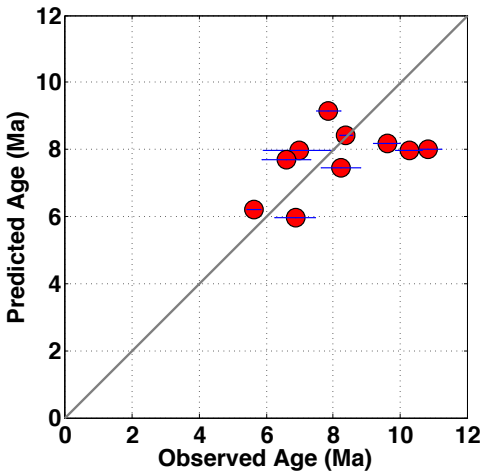

Figure 17 is a map of the landscape surface at Fjord Steffen, indicating the age of each point. **Figure 18** illustrates an age-elevation relationship for the observed ages of our samples and an age-elevation relationships for the predicted ages of our samples based on the simulation results. **Figure 19** is a plot of the observed age versus the predicted age for each sample location. The blue lines represent standard error bars.

Figure 20

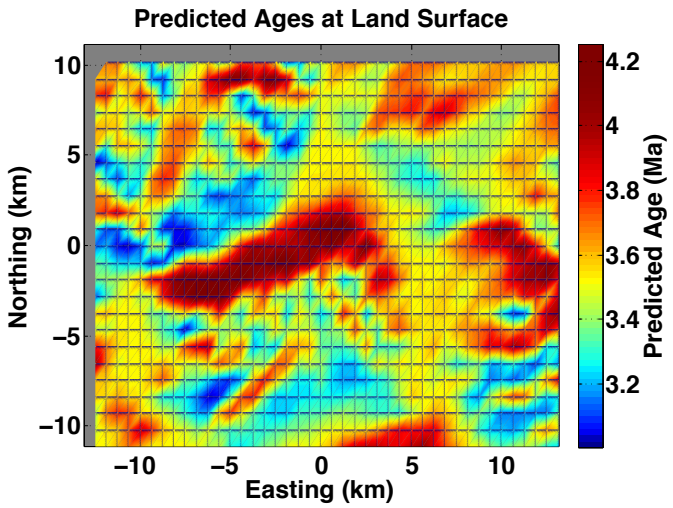

Figure 21

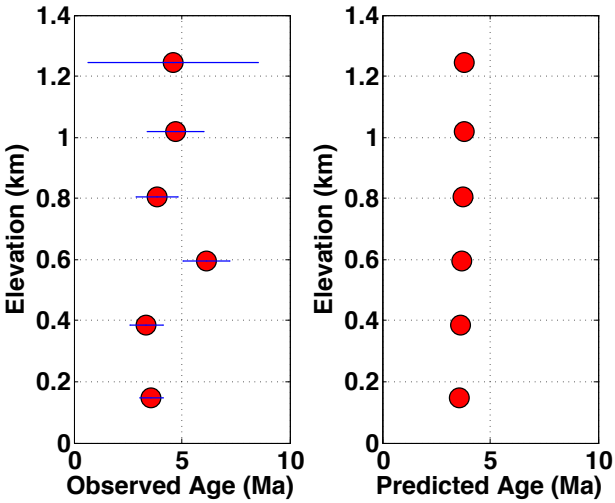

Figure 22

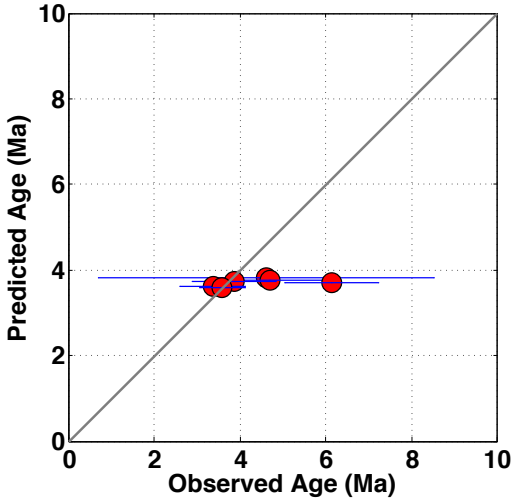

Figure 20 is a map of the landscape surface at East Cordon los Nadis, indicating the age of each point. **Figure 21** illustrates an age-elevation relationship for the observed ages of our samples and an age-elevation relationships for the predicted ages of our samples based on the simulation results. **Figure 22** is a plot of the observed age versus the predicted age for each sample location. The blue lines represent standard error bars.

Figure 23

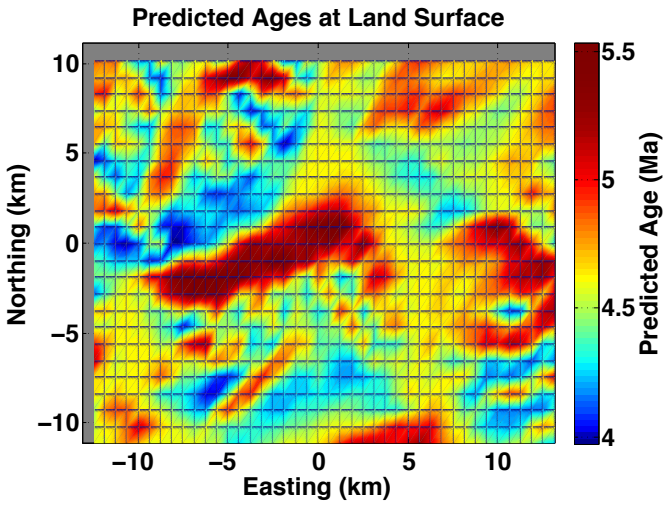

Figure 24

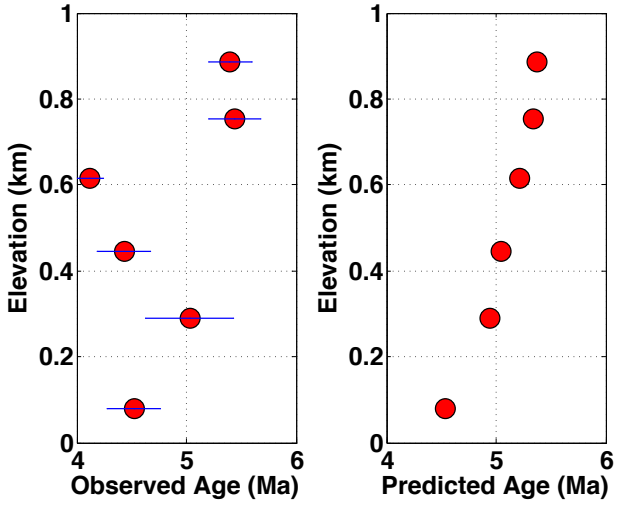

Figure 25

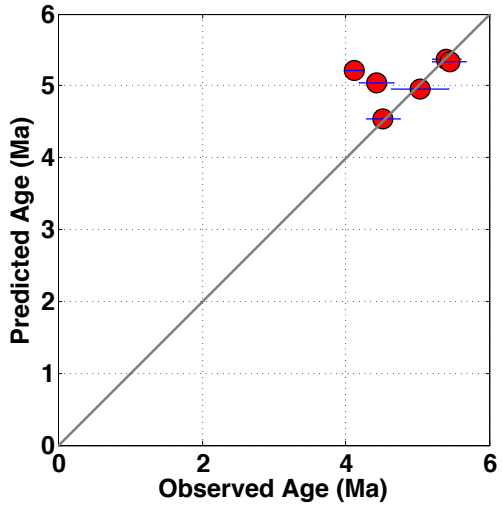

Figure 23 is a map of the landscape surface at North Cordon los Nadis, indicating the age of each point. **Figure 24** illustrates an age-elevation relationship for the observed ages of our samples and an age-elevation relationships for the predicted ages of our samples based on the simulation results. **Figure 25** is a plot of the observed age versus the predicted age for each sample location. The blue lines represent standard error bars.

Discussion

Observed Age-Elevation Relationships

The age-elevation relationships for our observed samples reveal a scattered plot. If the closure isotherm were flat, then the age would only correlate with vertical uplift, generating a straight-line age-elevation profile given a constant exhumation rate. Our data clearly does not follow this pattern. Thus, we developed a model that considers the other extreme, assuming that that the closure isotherm exactly conforms to the topography. The model represents the system by switching the reference frame of the problem. In our model, downward erosion of a surface is represented as rock moving towards that surface, which is held fixed. The velocity vector of the rock is equivalent to the glacial erosion velocity.

The two-dimensional simulation elucidates the end member behavior for dynamic uplift. The rock velocity vector changes to simulate the lateral propagation of landform features, which describe the observed age-elevation plot. When the rock velocity vector is at 90° relative to the Gaussian surface (no lateral propagation), the isochrones are stacked directly above the closure isotherm. Age increases proportionally with elevation; the resulting age-elevation plot is a straight vertical line. When the angle of inclination is 0° (no vertical propagation), the age-elevation plot will be one point. If the rock velocity has an angle of inclination between 0° and 90°, the model includes lateral and vertical propagation. The resulting isochrones will be offset at the given angle. A negative angle of exhumation (at an angle to the left of the vertical axis) represents upstream rock uplift, parallel to the slope of the modern bedrock surface. Age initially increases with elevation along the sloped bedrock. When the topography reaches a constant elevation, there is a range of ages for that plateau. The resulting age-elevation plot is a 7-shaped curve. A positive angle of exhumation (at an angle to the right of the vertical axis) represents downstream rock uplift, across the slope of the modern bedrock surface. Age decreases with elevation along the first part of the sloped segment; halfway along the knickpoint, the age begins to increase with elevation. This results in a C-shaped age-elevation plot.

As a simplified simulation, the two-dimensional model makes critical assumptions that may influence the accuracy of these generalized patterns. The model assumes that the closure isotherm precisely resembles the bedrock surface, the bedrock surface does not change shape over time and thus each isochrones has the identical shape, and the velocity vector remains constant over time. In actuality, mimicry decreases exponentially with depth; the isotherm and the resulting isochrones are

smooth versions of the topography. As the topography changes, the shape of the closure isotherm changes. Consequently, each isochrones, which mimic the shape of the closure isotherm when it is formed, has a slightly distinct shape. Furthermore, while this simulation represents samples along the front of the overdeepenings, our observations are transects up the sides of the valley. In this way, the model does not exactly correspond to our data points.

The age-elevation plots from our collected samples were complicated curves that did not closely resemble the end-member cases of our two-dimensional model. The three-dimensional simulation allows us to apply the same analysis to the topography in our specific study area. The model elucidates the scatter of the data points in the age-elevation plot. The ultimate goal is to determine the velocity vector that resulted in the observed topography. Velocity vectors, including a horizontal component, a vertical component, and an azimuth, are plugged into the model and compared to the actual observed data results. The velocity vector corresponds to the behavior of the actual topography when the model closely reproduces the results of the observed data. Incorporating lateral propagation of landforms into the model produced a better fit for the observed ages.

The simulation is particularly effective at replicating the observed data at high and low elevations. At mid elevations, between 300 and 600 meters, the model seems less precise at reproducing the observed data. Generally, the model closely resembles the overall trend of the topography. To quantitatively evaluate the model, we calculated the standard deviation of the residual data points, the points that are not precisely on the 1-to-1 plot. For Fjord Steffen, the standard deviation is 1.7 Ma; for East Cordon los Ñadis, the standard deviation is 1.6 Ma; for North Cordon los Ñadis, the standard deviation is 0.7 Ma. These standard deviations are within reasonable ranges for geological time scales. Incorporating lateral propagation into the simulation of glacial erosion appears to account for the data in a more complete fashion than just considering vertical propagation alone.

The solutions to the model suggest that the ice sheet is moving slowly over a long period of time. The horizontal velocities in the simulations are 0.25 km/Ma, 0.18 km/Ma, and 0.3 km/Ma, revealing low rates of lateral propagation. This confirms the preliminary conclusions of Ma et al. (in review) that the glacier carved the relief at a slow rate. The vertical velocities indicate that the glacier also eroded vertically into the landscape at a slow rate, although at a slightly faster rate than horizontal propagation. The vertical velocities are 0.4 km/Ma, 0.65 km/Ma, and 0.85 km/Ma. The

incision rates are higher for Cordon los Ñadis than for Fjord Steffen, suggesting that the glacier had varying rates of incision across the region.

The glacial erosion resulted in northward propagation of landform features. In the model, northward propagation of a topographic feature is equivalent to southward rock velocity with respect to the surface. The propagation direction (azimuth) ranges from 175° to 178°, indicating southward rock velocity and thus northward topographic propagation. As the glacier carved the overdeepening, the regressive knickpoint propagated from south to north. Because Fjord Steffen extends directly North to South, an azimuth of about 180° is a reasonable solution. The two transects at Cordon Los Ñadis are on different sides of the mountain and thus located in different valleys. Accordingly, the two transects have slightly different azimuths.

To quantitatively evaluate the similarity and consistency between the three solutions, the residual standard deviations for each solution were combined. The resulting standard deviation of combining the Cordon los Ñadis solutions was a standard deviation of 1.1 Ma, suggesting that the models are reasonably congruent. This consolidated Cordon los Ñadis residuals standard deviation was combined with the residual standard deviation for Fjord Steffen. The resulting standard deviation of 1.3 Ma was within an appropriate range to confirm that the models closely correspond.

$$\sigma_{ab}^2 = [\sigma_a^2*(n_a-m_a)+\sigma_b^2*(n_b-m_b)]/(n_a+ n_b- 4)$$

Cordon los Ñadis Solutions: $[1.6^2 *(6-3) + 0.7^2*(6-3)]/(6+6-4) = 1.14 \rightarrow \sigma_{ab} = 1.1$ Ma

Cordon los Ñadis + Steffen Solutions:

$[1.07^2 *(12-3) + 1.7^2*(10-3)]/(12+10-4) = 1.69 \rightarrow \sigma_{ab} = 1.3$ Ma

The presence of old cooling ages at the surface suggests that glacial erosion was relatively slow. In the Fjord Steffen transects, the weighted averages for three of the samples are greater than 10 Ma, including 10.09, 10.28, and 10.89 Ma. This supports the idea of glacial protection that Thomson et al. (2010) proposed. The slow, restricted movement of the warm-based glacier preserved the landscape similar to cold-based glaciers that do not slide at all. This suggests that the glacier is not adequately erosive to drive the glacial buzzsaw effect, as Thomson et al. (2010) argued.

Conclusion

This study determined a new understanding of the thermal history of the Central Patagonian Andes was determined. A two-dimensional simulation demonstrates that, for a thermochronometric system with a shallow closure temperature, lateral propagation of landforms is an essential factor for understanding age-elevation relationships. The effect of lateral propagation was incorporated into a new three-dimensional model to elucidate the age-elevation relationships for samples collected in the Caleta Tortel study area. The model reveals that overdeepenings were incised at slow rates with topographic features propagating northward. The limited movement of the glacier resulted in landscape preservation, indicated by the presence of old surface bedrock. This further suggests that the glacial buzzsaw effect is not active in this region.

Acknowledgements

I would like to thank profoundly Mark T. Brandon for mentoring me for the past three years. Mark not only advised me on this project but also has been my primary academic guide throughout my Yale career. Mark is the primary reason that I became interested in geology and the processes that shape the earth. I am very grateful to have worked with and learned from him. This thesis is the culmination of many semesters of work on this topic. I began researching the geology of the Andes under the guidance of Mark in my first geology class, Global Tectonics, in my freshman year. In sophomore year, I wrote my final paper on the glacial buzzsaw in Earth System Science. I started the research for this senior thesis in the fall of my junior year. Thank you for your incredible dedication to me as a student.

I would like to thank Elizabeth Christeleit for all the help she gave to make this a successful project. I have learned so much from Liz in the past two years that we have worked on this project together – from how to break a piece of bedrock off with a rock hammer to the details of correcting ages in broken apatite grains. Her patience for teaching me key concepts is remarkable. Moreover, I am indebted to her for completing preparation of samples and going to Berkeley to date the samples.

I would like to thank Ryan Laemel for being an incredible research partner. From climbing mountains in Patagonia to crushing rocks in the rock lab, we have been on an amazing adventure together.

I would like to thank our Chilean guide, Noel, for leading us off-trail to the summits of the peaks in Fjord Steffen. We would never have completed the transects without him.

I would also like to acknowledge John Garver and David Shuster for letting us use their facilities and helping us with the data analysis.

Thank you to the Karen Von Damm Memorial Scholarship, the department of Geology and Geophysics, and the office of the Dean of Science and Engineering for providing us with funding to pursue field work in Patagonia.

References Cited

Braun, Jean, Peter Van der Beek, Geoffrey Batt. *Quantitative Thermochronology: Numerical methods for the interpretation of thermochronological data*. Cambridge University Press.

Braun, Jean. Quantifying the effect of recent relief changes on age-elevation relationships. Earth and Planetary Science Letters 200: 331-343 (1 April 2002).

Brozovic, Burbank, and Meigs. Climatic Limits on Landscape Development in the Northwestern Himalaya. *Science* 276, 471-574 (1997).

Dodson, Martin H. Closure Temperature in Cooling Geochronological and Petrological Systems. Contr. Mineral. And Petrol. 40, 259-274 (5 March 1973)

Egholm, D. L., S.B. Nielsen, V.K. Dersen and J.E. Lesemann. Glacial effects limiting mountain height. *Nature* vol 460, pp 884-887 (13 August 2009).

Ehlers, Todd A. and Kenneth A. Farley. Apatite (U-Th)/He thermochronometry: methods and applications to problems in tectonic and surface processes. *Earth and Planetary Science Letters* (5 Nov 2002).

Farley K. A. R.A. Wolf and LT Silver. The effects of long alpha-stoping distances on (U-Th)/He ages. Geochimica et Cosmochimicia Acta, Vol 60, no 21, pp 4223-4229 (June 8, 1996).

Ma, K., Roe, G., Brandon, M., 2012, Ice cap glaciation and formation of a deeply incised glacial landscape beginning by ~6 Ma in Patagonia, In Review.

McPhillips, Devin and Mark T. Brandon. "Using tracer thermochronology to measure modern relief change in the Sierra Nevada, California. *Earth and Planetary Science Letters* (18 May 2010).

Mercer J.H. and J.F. Sutter. "Late Miocene-Earliest Pliocene Glaciation in Southern Argentina: Implications for Global Ice-Sheet History." *Palaeogeography, Palaeoclimatology, Palaeoecology*, 38: 185-206 (July 1982).

Reiners, Peter W. and Mark T. Brandon. Using Thermochronology to Understand Orogenic Erosion. Annual Review of Earth and Planetary Science. 34: 219-66 (16 January 2006).

Shuster, David L., Kurt. M. Cuffey, Johnny W. Sanders, Greg Balco. Thermochronmetry Reveals headward propagation of erosion in an alpine landscape. Science Vol 332 pg 84-88. (1 April 2011)

Smith R.B. and J.P. Evans. "Orographic Precipitation and Water Vapor Fractionation over the southern Andes." *Journal of Hydrometeorology* 8.1: 3-19 (February 2007).

Thomson, S.N., Brandon, M.T., Tomkin, J.H., Reiners, P.W., Vásquez, C., and Wilson, N.J., 2010, Glaciation as a destructive and constructive control on mountain building: Nature, v. 467, no. 7313, p. 313-7.

Wendy De Wolf
Morse College
Class of 2014

Investigating the Glacial and Topographic History of the Central Patagonian Andes using (U-Th)/He Thermochronology

Appendix

Figure 1: Fjord Steffen, view from the northwest peak

Figure 2: Collecting granite samples at Fjord Steffen

Matlab Code for the two-dimensional simulation:


```
function sim2D
%% Initialize system
clear all
close all
clc
dbstop if error
%% set up variables
w = 1; % vertical rock velocity
u = 0; % horizontal rock velocity
width = 12;
relief = 2;
zC = 3;% closure depth
zMin = -relief - zC -1;
zMax = relief+2;
xMin = -20;
xMax = 20;
xzStep = 0.1;
rX = (xMin:xzStep:xMax)';% bedrock surface, x component
rZ = -relief*(2*normcdf(rX,0,width/6)-1);% bedrock surface, z component
sX = rX;%closure surface
sZ = rZ - zC;
[X,Z] = meshgrid(xMin:xzStep:xMax,zMin:xzStep:zMax);
ageStep = 1;
ageMin = floor(((-2*relief -1)/w)/ageStep)*ageStep;
ageMax = ceil(((zC + 2*relief + 2)/w)/ageStep)*ageStep;
nAgeStep = (ageMax-ageMin)/ageStep;
cX = zeros(length(rX),(nAgeStep+1));
cZ = cX;
cAge = cX;
%% Make calculation
for i=0:nAgeStep
    age = ageMin +i*ageStep;
    dX = age*u;
    dZ = age*w;
    cX(:,i+1) = rX;
    cZ(:,i+1) = dZ - zC - relief*(2*normcdf(rX,-dX,width/6)-1);
    cAge(:,i+1 ) = age*ones(size(rX));
end
%... Intepolate for gridded isochrone ages
F = TriScatteredInterp(cX(:),cZ(:),cAge(:));
C_Age = F(X,Z);
%... Interpolate for bedrock surface ages
cAgeBedrock = interp2(X,Z,C_Age,rX,rZ);
%... Clip isochrone grid so that only values between
% the closure surface and the topographic surface are retained.
```

```
46 C_Age(C_Age<-0.01) = nan;
47 C_Age(Z > repmat(rZ',size(Z,1),1)+0.01) = nan;
48 %% Plot figures
49 figure(1)
50 hold on
51 plot(cX,cZ,'-b','LineWidth',2);
52 plot(rX,rZ,'-k','LineWidth',2);
53 plot(sX,sZ,'-r','LineWidth',2);
54 plot([xMin,xMin,xMax,xMax,xMin], ...
55     [zMin,zMax,zMax,zMin,zMin], '-g','LineWidth',2);
56 axis equal
57 title('  Contoured Isochrones  ')
58 xlabel('  Horizontal Distance (km)  ')
59 ylabel('  Elevation (km)  ')
60 figure(2)
61 hold on
62 pcolor(X,Z,C_Age)
63 shading interp
64 colormap(jet(256));
65 %colormap(hot)
66 h = colorbar;
67 ylabel(h,'Isochrone Age (Ma)');
68 plot(rX,rZ,'-k','LineWidth',1);
69 plot(sX,sZ,'-r','LineWidth',3);
70 xlim([xMin,xMax]);
71 ylim([zMin,zMax]);
72 title('  Continuous Isochrones  ')
73 xlabel('  Horizontal Distance (km)  ')
74 ylabel('  Elevation (km)  ')
75 figure(3)
76 plot(cAgeBedrock, rZ,'ro','MarkerSize',16)
77 title('Age-Elevation Relationship')
78 xlabel('Age (Ma)')
79 ylabel('Relief (km)')
80 xlim([0,5])
81 axis square
82 end
83 % sim2D was written by Mark Brandon and Wendy De Wolf, Yale University, Spri
```

Matlab Code for the three-dimensional simulation:


```
function sim3D_Steffen
%% Initialize system
clear all
close all
clc
dbstop if error

%% User variables
%... Select file for age data
agesInputFile = 'PatagonianAndesThermochronData_MTB.txt';
%... Select type of ages: 1=ARB, 2=FTZ, 3=HEZ, 4=FTA, 5=HEA
jMethod = 5;
%... Select grid file
gridInputFile = 'Steffan.nc';
%... Set velocities
vel = 0.3;    % magnitude (km/Ma) for horizontal rock velocity
azim = 175;   % azimuth for horizontal rock velocity
w = 0.4;     % vertical rock velocity (corresponds with z)

%% Program variables (no changes needed here)
u = vel*sind(azim); % east component of rock velocity (corresponds with x)
v = vel*cosd(azim); % north component of rock velocity (corresponds with y)
zC = 3; % closure depth
ageStep = 0.25;
zStep = 0.25;
method = {'ARB';'FTZ';'HEZ';'FTA';'HEA'};
cm2pt = 3*28.3464567; % convert cm to points

%% Input GMT map data
[lon,lat,H]=grdread(gridInputFile);
lonMean = mean(lon);
latMean = mean(lat);
lat2km = 111.11;
lon2km = 111.11*cosd(mean(lat));
lonMin = lon(1);
lonMax = lon(end);
latMin = lat(1);
latMax = lat(end);
x = (lon-lonMean)*lon2km; % easting
y = (lat-latMean)*lat2km; % in distances not degrees, northing
[X,Y]= meshgrid(x,y); % x and y are now gridpoints (instead of vectors)
H = H/1000; % elevations in km
hMin = min(H(:)); % minimum elevation
hMax = max(H(:)); % maximum elevation
%... Elevation of closure surface
```

```
% hMean option gives a flat closure surface
%hMean = mean(H(:)); % mean elevation
%S = hMean-zC;
% H option gives a closure surface that follows the topography
S = H - zC;

%% Input age data for Patagonian Andes
tab = char(9);
fid0=fopen(agesInputFile,'r');
nSample=0;
while ~feof(fid0)
    recLine = fgetl(fid0);
    if isempty(recLine) || recLine(1) ~= '#'
        tabPositions=strfind(recLine,tab);
        lon = str2double(recLine(1:tabPositions(1)-1));
        lat = str2double(recLine(tabPositions(1)+1:tabPositions(2)-1));
        methodSample = strtrim(recLine(tabPositions(5)+1:tabPositions(6)-1))
        if lonMin<=lon && lonMax>=lon ...
                && latMin<=lat && latMax>=lat ...
                && strcmp(methodSample,method(jMethod))
            nSample = nSample+1;
            lonSample(nSample) = lon;
            latSample(nSample) = lat;
            hSample(nSample) = str2double(recLine(tabPositions(2)+1:tabPosit
            hSample(nSample) = hSample(nSample)/1000; %... Convert to kilome
            ageSample(nSample) = str2double(recLine(tabPositions(3)+1:tabPos
            seAgeSample(nSample) = str2double(recLine(tabPositions(4)+1:tabP
            nameSample{nSample} = strtrim(recLine(tabPositions(6)+1:end));
        end
    end
end

%... Convert sample lon, lat to x,y
xSample = (lonSample-lonMean)*lon2km;
ySample = (latSample-latMean)*lat2km;

%% Start calculation
%... Find vertical limits for calculated isochrones
zMin = floor((hMin - zC - zStep)/zStep)*zStep;
zMax = ceil((hMax + zStep)/zStep)*zStep;
nX = length(x);
nY = length(y);
%... Find age limits for calculated isochrones
ageMin = floor((((zMin-(hMax-zC))/w)/ageStep))*ageStep;
ageMax = ceil((((zMax-(hMin-zC))/w)/ageStep))*ageStep;
```

```
91  nAgeStep = ceil((ageMax-ageMin)/ageStep);
92  %... Set nodes in S to nan that initially propogate downward from closure su
93  F = scatteredInterpolant(X(:), Y(:), S(:),'linear','none');
94  S(S + ageStep*w/10 < F(X + ageStep*u/10, Y + ageStep*v/10)) = nan;
95  %... Initial arrays for predicted ages
96  cX = zeros(nY,nX,(nAgeStep+1));
97  cY = cX;
98  cZ = cX;
99  cAge = cX;
100 % Calculate ages for grid
101 for i=0:nAgeStep
102     age = ageMin + i*ageStep;
103     dX = age*u;
104     dY = age*v;
105     dZ = age*w;
106     cX(:,:,i+1) = X + dX;
107     cY(:,:,i+1) = Y + dY;
108     cZ(:,:,i+1) = S + dZ;
109     cAge(:,:,i+1) = age*ones(nY,nX);
110 end
111 %... Remove nans
112 iGood = repmat(~isnan(S),1,1,size(cX,3));
113 cX = cX(iGood);
114 cY = cY(iGood);
115 cZ = cZ(iGood);
116 cAge = cAge(iGood);
117 %... Intepolate for gridded isochrone ages
118 F = scatteredInterpolant(cX,cY,cZ,cAge,'linear','none');
119 C_Age = F(X,Y,H);
120
121 %... Calculate predicted ages
122 ageSamplePredicted = F(xSample,ySample,hSample);
123
124 %... Calculate standard deviation of the residuals
125 sdResidual = ...
126     sqrt(sum((ageSample - ageSamplePredicted).^2)./(nSample-3));
127
128 %% Report results
129 fprintf('======================== Summary of Fit ========================\n'
130 fprintf('File for age data: %s\n', agesInputFile);
131 fprintf('File for grid data: %s\n', gridInputFile);
132 fprintf('Age method: %s\n',method{jMethod});
133 fprintf('Standard deviation of residuals (Ma): %5.1f\n',sdResidual);
134 fprintf('Number of ages:                       %5d\n',nSample);
135 fprintf('Number of fit parameters:             %5d\n',3);
```

```
136 fprintf('\n============== Details on Isochrone Calculation ==============\n'
137 fprintf('Percentage of downward-propagating points: %5.1f\n', ...
138     100*(1-sum(iGood(:))/numel(iGood)));
139 fprintf('Percentage of out-of-bound points: %5.1f\n', ...
140     100*(1-sum(isnan(C_Age(:))/numel(C_Age))));
141 
142 %% Plot figures
143 figure(1)
144 %... Predicted ages at land surface
145 hold on;
146 set(gca,'color',[0.5 0.5 0.5]);
147 pcolor(X,Y,C_Age);
148 shading interp;
149 cpmap = jet;
150 cpmap = cmapscale(H,cpmap,1);
151 colormap(cpmap);
152 grid on;
153 axis equal tight
154 title('  Predicted Ages at Land Surface  ');
155 xlabel('Easting (km)');
156 ylabel('Northing (km)');
157 h = colorbar; % h is a handle
158 ylabel(h,'  Predicted Age (Ma)  ');
159 
160 figure(2)
161 plot(C_Age,H,'ro','MarkerSize',16)
162 title('  Elevation vs. Predicted Surface Ages  ')
163 xlabel('  Predicted Age (Ma)  ')
164 ylabel('  Elevation (km)  ')
165 axis square
166 
167 figure(3)
168 %... Sample map with topography
169 hold on
170 pcolor(X,Y,H);
171 shading interp;
172 % Adjust so use color values evenly across map. 1 means it is done by area
173 cpmap = haxby;% color scheme
174 cpmap = cmapscale(H,cpmap,1);
175 colormap(cpmap);
176 %... Plot samples
177 for i=1:nSample
178     switch jMethod
179         case 1
180             %... ARB, 0.40c black cross
```

```
            plot(xSample(i),ySample(i),'xk', ...
                'MarkerSize', 0.40*cm2pt, 'MarkerFaceColor',[0 0 0]);
        case 2
            %... FTZ, 0.35c blue square
            plot(xSample(i),ySample(i),'sk', ...
                'MarkerSize', 0.35*cm2pt, 'MarkerFaceColor',[0 0 1]);
        case 3
            %... HEZ, 0.30c turquoise circle
            plot(xSample(i),ySample(i),'ok', ...
                'MarkerSize', 0.30*cm2pt, 'MarkerFaceColor',[0 0.8 0.8]);
        case 4
            %... FTA, 0.20c light orange circle
            plot(xSample(i),ySample(i),'ok', ...
                'MarkerSize', 0.20*cm2pt, 'MarkerFaceColor',[1 0.6 0]);
        case 5
            %... HEA, 0.10c red circle
            plot(xSample(i),ySample(i),'ok', ...
                'MarkerSize', 0.20*cm2pt, 'MarkerFaceColor',[1 0 0]);
    end
end
grid on;
axis equal tight
xlabel('  Easting (km)  ');
ylabel('  Northing (km)  ');
h = colorbar;
ylabel(h,'  Elevation (km)  ');

figure(4)
%... Plot observed  and predicted ages vs elevation
subplot(1,2,1)
%... Observed age vs elevation
hold on
for i=1:nSample
    switch jMethod
        case 1
            %... ARB, 0.40c black cross
            plot(ageSample(i),hSample(i),'xk', ...
                'MarkerSize', 0.40*cm2pt, 'MarkerFaceColor',[0 0 0]);
        case 2
            %... FTZ, 0.35c blue square
            plot(ageSample(i),hSample(i),'sk', ...
                'MarkerSize', 0.35*cm2pt, 'MarkerFaceColor',[0 0 1]);
        case 3
            %... 0.30c turquoise circlek
            plot(ageSample(i),hSample(i),'ok', ...
```

```
                'MarkerSize', 0.30*cm2pt, 'MarkerFaceColor',[0 0.8 0.8]);
        case 4
            %... FTA, 0.20c light orange circle
            plot(ageSample(i),hSample(i),'ok', ...
                'MarkerSize', 0.20*cm2pt, 'MarkerFaceColor',[1 0.6 0]);
        case 5
            %... HEA, 0.10c red circle
            plot(ageSample(i),hSample(i),'ok', ...
                'MarkerSize', 0.20*cm2pt, 'MarkerFaceColor',[1 0 0]);
            hold on
            herrorbar(ageSample(i), hSample(i), 4*seAgeSample(i));
    end
end
h1 = gca;
xl1 = xlim;
yl1 = ylim;
grid on;
xlabel('  Observed Age (Ma)  ');
ylabel('  Elevation (km)  ');

subplot(1,2,2)
%... Predicted ages vs elevation
hold on
for i=1:nSample
    switch jMethod
        case 1
            %... ARB, 0.40c black cross
            plot(ageSamplePredicted(i),hSample(i),'xk', ...
                'MarkerSize', 0.40*cm2pt, 'MarkerFaceColor',[0 0 0]);
        case 2
            %... FTZ, 0.35c blue square
            plot(ageSamplePredicted(i),hSample(i),'sk', ...
                'MarkerSize', 0.35*cm2pt, 'MarkerFaceColor',[0 0 1]);
        case 3
            %... HEZ, 0.30c turquoise circle
            plot(ageSamplePredicted(i),hSample(i),'ok', ...
                'MarkerSize', 0.30*cm2pt, 'MarkerFaceColor',[0 0.8 0.8]);
        case 4
            %... FTA, 0.20c light orange circle
            plot(ageSamplePredicted(i),hSample(i),'ok', ...
                'MarkerSize', 0.20*cm2pt, 'MarkerFaceColor',[1 0.6 0]);
        case 5
            %... HEA, 0.10c red circle
            plot(ageSamplePredicted(i),hSample(i),'ok', ...
                'MarkerSize', 0.20*cm2pt, 'MarkerFaceColor',[1 0 0]);
```

```
    end
end
h2 = gca;
xl2 = xlim;
yl2 = ylim;
grid on;
xlabel('  Predicted Age (Ma)  ');
ylabel('  Elevation (km)  ');

%... Scale plots so that they have the same ranges
xl1(1) = min([xl1(1),xl2(1)]);
xl1(2) = max([xl1(2),xl2(2)]);
yl1(1) = min([yl1(1),yl2(1)]);
yl1(2) = max([yl1(2),yl2(2)]);
subplot(1,2,1)
xlim(h1,xl1);
ylim(h1,yl1);
subplot(1,2,2)
xlim(h2,xl1);
ylim(h2,yl1);

figure(5)
%... Plot predicted ages vs observed ages with 1:1 reference line
hold on
for i=1:nSample
    switch jMethod
        case 1
            %... ARB, 0.40c black cross
            plot(ageSample(i),ageSamplePredicted(i),'xk', ...
                'MarkerSize', 0.40*cm2pt, 'MarkerFaceColor',[0 0 0]);
        case 2
            %... FTZ, 0.35c blue square
            plot(ageSample(i),ageSamplePredicted(i),'sk', ...
                'MarkerSize', 0.35*cm2pt, 'MarkerFaceColor',[0 0 1]);
        case 3
            %... HEZ: 0.30c turquoise circle
            plot(ageSample(i),ageSamplePredicted(i),'ok', ...
                'MarkerSize', 0.30*cm2pt, 'MarkerFaceColor',[0 0.8 0.8]);
        case 4
            %... FTA, 0.20c light orange circle
            plot(ageSample(i),ageSamplePredicted(i),'ok', ...
                'MarkerSize', 0.20*cm2pt, 'MarkerFaceColor',[1 0.6 0]);
        case 5
            %... HEA, 0.10c red circle
            plot(ageSample(i),ageSamplePredicted(i),'ok', ...
```

```
316                 'MarkerSize', 0.20*cm2pt, 'MarkerFaceColor',[1 0 0]);
317             hold on
318             herrorbar(ageSample(i), ageSamplePredicted(i), 4*seAgeSample(i)
319     end
320 end
321 %... Draw 1:1 reference line
322 xl = xlim;
323 yl = ylim;
324 maxPoint = max([xl(2),yl(2)]);
325 plot([0,maxPoint],[0, maxPoint], '-', ...
326     'LineWidth',2,'Color',[0.5 0.5 0.5]);
327 axis equal
328 xlim([0,maxPoint]);
329 ylim([0,maxPoint]);
330 grid on;
331 xlabel('  Observed Age (Ma)  ');
332 ylabel('  Predicted Age (Ma)  ');
333
334 % sim3D was written by Mark Brandon and Wendy De Wolf, Yale University, Spr
335
336
```